Available online at www.sciencedirect.com

ScienceDirect

journal homepage: www.elsevier.com/locate/he

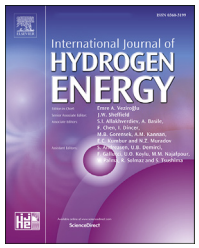

Automized parametrization of PEM and alkaline water electrolyzer polarisation curves

Lauri Järvinen [a,*], *Pietari Puranen* [a], *Antti Kosonen* [a], *Vesa Ruuskanen* [a], *Jero Ahola* [a], *Pertti Kauranen* [a], *Michael Hehemann* [b]

[a] *Lappeenranta-Lahti University of Technology, P.O. Box 20, FI-53851, Lappeenranta, Finland*
[b] *Forschungszentrum Jülich, Wilhelm-Johnen-Straße, DE-52428, Jülich, Germany*

HIGHLIGHTS

- Critical review of the water electrolyzer polarisation curve modelling is conducted.
- Open source MATLAB toolbox for automated parametrization of models is presented.
- Measured alkaline and PEM water electrolyzer data is used to verify fit accuracy.
- Data sets of variable quality are used to verify fitting robustness.

ARTICLE INFO

Article history:
Received 14 April 2022
Received in revised form
8 June 2022
Accepted 10 July 2022
Available online 2 September 2022

Keywords:
Water electrolyzer modelling
PEM water electrolysis
Alkaline water electrolysis
Hydrogen

ABSTRACT

A comprehensive literature review of current water electrolyzer modelling research was conducted and presented models critically evaluated. Based on the literature review this paper presents an open-source MATLAB toolbox for water electrolyzer polarisation curve parametrization and modelling. The modelling capabilities of the tooling were verified using measured PEM and alkaline water electrolyzer polarisation data. As real-world measurement data is rarely ideal, tests were also conducted using suboptimal data, first with data sets that have a low number of measurement points and secondly with data sets that have low or high current densities missing. The tooling is shown to work with a wide variety of use cases and provides an automated method for modelling and parametrization of electrolyzer polarisation curves.

Introduction

Hydrogen is likely to play a major role in future energy systems in limiting the increase in global mean temperature, in accordance with the Paris Agreement, below 1.5 °C compared to pre-industrial levels [1]. In the energy transition, large amounts of CO_2-free power generation have to be implemented to replace old fossil fuel-based generation facilities. However, CO_2-free power generation would limit energy sources mainly to wind and solar, which are by their nature intermittent. Intermittency of power production can lead to an imbalance between generation and consumption, which means that flexible consumption is needed for times of overproduction and effective energy storage solutions for times of underproduction. Water electrolyzer produced

* *Corresponding author.*
E-mail address: lauri.jarvinen@lut.fi (L. Järvinen).
https://doi.org/10.1016/j.ijhydene.2022.07.085

Nomenclature

Variables

a_X	Activity of reagent X
α	Electron transfer coefficient
a	Tafel slope
A	Active surface area
C_X	Reagent X concentration
$C_{X,0}$	Reagent X concentration in reference working conditions
δ	Electrolyte layer thickness
ΔG	Gibbs free energy change
η_F	Faraday efficiency
j	Current density
j_0	Exchange current density
j_0^*	Constant base exchange current density value
$j_0^\dagger$	Multiplier depicting the change in j_0
j_L	Limiting current density
λ	Membrane water content
m	Molality
M	Molarity
$\dot{n}_{H_2}$	Generation rate of hydrogen
n_e	Number of electrons transferred in a unit electrochemical reaction
ν_X	Stoichiometric coefficient of reagent X
O	General chemical species oxidized in the reaction
p_X	Partial pressure of reagent X
p_{sv}	Saturated vapor pressure in pure water
$p_{sv,el}$	Saturated water vapor pressure in electrolyte
p°	Standard reference pressure of 1 bar
r_e	Electric area specific resistance
R	General chemical species reduced in the reaction
r_i	Ionic area specific resistance
ρ	Material resistivity
σ	Material conductivity
T	Temperature (in kelvin)
U_{act}	Activation overpotential
U_{cell}	Cell voltage
U_{con}	Concentration overpotential
U_{ohm}	Ohmic overpotential
U_{ocv}	Open circuit voltage
U°	Temperature-dependent reference voltage
w	Mass fraction

Subscript

a	Anode
c	Cathode

Acronyms

AWE	Alkaline Water Electrolyzer
OCV	Open Circuit Voltage
PEM	Proton Exchange Membrane
PEMWE	PEM Water Electrolyzer
SEC	Specific Energy Consumption

Constants

F	Faraday's constant
$\mathcal{R}$	Universal gas constant

hydrogen is considered one of the most promising options for overcoming both problems. Water electrolyzers could convert the produced electricity to chemical energy in the form of hydrogen, which can then be transformed back to electricity with a fuel cell. Hydrogen can be used in many applications and can play a important role in the energy transition by indirectly electrifying sectors of society where direct electrification is unlikely to be feasible in the near future. Renewable energy production is possible in all parts of the world and when combined with a sustainable energy storage solution can enable an increase in energy self-sufficiency and a reduction in reliance on imported fossil fuels.

Electrolyzer research and development makes extensive use of modelling to explore electrolysis phenomena and examine the sizing, energy management, control analysis, and optimisation of electrolyzer plants. Consequently, various models of varying degrees of complexity have been produced for a wide range of different applications of water electrolyzer research. In recent years, a number of valuable reviews of electrolyzer modelling have been published. For example, the reviews focusing on the proton exchange membrane water electrolyzer (PEMWE) by Falcao et al. [2] and Hernández-Gómez et al. [3]. For low-temperature water electrolysis system modelling in general, the work by Olivier et al. [4], provides a very complete review with each model classified according to criteria such as modelling approach and included overpotentials. Furthermore, recent review by Gambou et al. [5] concentrated on the electrical domain of alkaline water electrolysis modelling. They noted that static models are well developed but dynamic modelling has not seen same kind of attention. Although these publications present a good overview of the landscape of water electrolyzer modelling, the scope of these publications does not include rigorous evaluation of the fundamentals of the modelling equations. A modelling review where the theoretical background of the equations is critically assessed is missing from the literature.

Electrolyzer modelling is currently divided into three different approaches: analytical, empirical or semi-empirical, and mechanistic approaches. Analytical models can be used to determine the effect of the main variables on electrolyzer performance, using simplifications to simulate a fairly accurate polarisation curve [2]. Research using an analytical approach has tended to focus on PEMWE modelling. For example Abdin et al. [6] presented a linked modular mathematical model. The model was constructed using modular models for the anode, cathode, membrane, and cell voltage. In addition to prediction of the equilibrium electrolyzer cell performance, the model can also be used to study control strategies and to understand the contribution of various internal components to cell voltage. In a recent PEMWE modelling publication Correa et al. [7] presented a lumped dynamic model focusing on the cathode side to predict the

electrolyzer performance. They found out that temperature increase mainly affects the ohmic overpotential while increasing the cathode pressure leads to rise in the cathode activation overpotential. Choi et al. [8] conducted an analysis of PEMWE using a simple model based on Butler-Volmer kinetics. The model can be used to analyse the individual resistances of each electrolysis process step in the membrane and electrode unit and to predict overpotentials with different electrocatalysts. García-Valverde et al. [9] proposed a model for simulating the electrochemical, thermal, and H_2 output flow behaviours. They noted that the electrochemical model could be extrapolated for any PEMWE based on knowledge of the activation energy of the water oxidation reaction for the anode electrocatalyst and the energy for proton transport in the PEM. Few analytical models are available for alkaline water electrolyzer (AWE) modelling. One such model is the multiphysics-based approach for modelling and design of AWE presented by Hammoudi et al. [10]. The model includes characterisation based on structural and operational parameters, which allows it to describe a range of AWE. A similar model has also been developed by Henao et al. [11] whose model focuses on separately modeling the physical effects taking place in the electrolyzer cell.

Empirical models use measurements from an electrolyzer to determine the equation parameters used in the models. The main disadvantage of empirical models is that they are usually limited to the specific electrolyzer design used for model design and the operation conditions studied. The work by Koponen et al. [12] presented a semi-empirical model that could be used to study the effect of power quality on the specific energy consumption of a PEMWE. Dale et al. [13] modelled a 6 kW PEMWE using semi-empirical equations. They included a temperature and pressure dependant Nernst potential and emphasised the importance of the temperature dependency for achieving accurate results. The work by Ulleberg et al. [14] has been widely used in empirical methods-based AWE modelling. The model is based on a combination of heat transfer theory, fundamental thermodynamics, and empirical electrochemical relationships. The model can be used to predict various system parameters such as cell voltage, efficiency, and hydrogen production. Recent dynamic energy and mass balance model for industrial scale alkaline water electrolyzer has been published by Sakas et al. [15]. The model was verified with measurement data from a similarly sized industrial plant. Based on their modelling, shunt currents were observed to be the main contributor for the low faradaic efficiency of the studied plant.

Mechanistic models use differential and algebraic equations derived from electrochemical phenomena occurring in the electrolyzer. These models require extensive calculations to produce very accurate predictions of the polarisation curve and the flux concentration of multiple species in the electrolyzer. Due to the number of calculations needed, simulation times are, however, significantly slower than those of analytical or empirical models. Bree et al. [16] developed a mechanistic dynamic model for comparing different cell setups. Overpotentials caused by ohmic losses and mass transport limitations were included to show their effect at high current densities, and gas bubble formation was taken into account via geometrical considerations and experimental data. The work notes that one major limitation for PEM cells is the formation of bubbles and proposes that a higher gas diffusion layer porosity and change from a liquid to gaseous inlet stream could be a solution. Onda et al. [17] used measured overpotentials to make a two-dimensional simulation, which was used to predict the performance of a large-scale PEMWE. Additionally, by using the model, it was possible to show that the potential used for water electrolysis stays constant along the water flow direction. Chanderis et al. [18] created a 1D PEMWE model that incorporated chemical degradation of the membrane for degradation studies. The model was used to capture the effects of temperature and current density on the degradation rates. A fluid dynamic based model was presented by Ma et al. [19] including an ANSYS based tool for using it. They noted that the benefit of fluid dynamic based model is the ability to model phase, current, and temperature distributions in an operating electrolysis cell which are difficult or impossible to measure.

In this work, we take a critical look at modelling and parametrization of water electrolyzers. A literature review is conducted in which the theory behind each model is evaluated and limitations listed. Based on this theoretical foundation, we develop a novel open-source modelling and parametrization tool for AWE and PEMWE. The tool allows models found in these literature sources to be easily combined together and also incorporates checking for model limitations that can affect the accuracy of the results. Implementation of additional models is made easy by design.

For parametrization of the models, the tool includes easy to use curve fitting for polarisation curve fits. Curve fittings are usually used to obtain values for model parameters that are difficult to measure or calculate analytically. Currently, most modelling tools such as MATLAB provide very generic fitting functionality, and a lot of setup work is consequently required before they can be used for water electrolyzer model parametrization. Our tool thus provides ready-made functions for parametrization of water electrolyzer polarisation curves, significantly reducing the time required for this repetitive task. Additionally, error bound calculations for each fitted parameter and for the resulting curve are also included when parametrization is performed.

The performance of the tooling is verified with data from a PEMWE at the Forschungszentrum Jülich, Germany and with an AWE at LUT University, Finland.

The novelty of this research is the critical literature review of the most popular water electrolyzer models, where the theoretical background is evaluated, and the limitations are listed and the automized parametrization tool is developed based on the literature review. The tool can automatically parametrize water electrolyzer models, using polarisation curve data, that are widely used in the literature based on measurement results. Confidence interval is also automatically calculated for each parameter value. All this functionality is packaged into an open source MATLAB toolbox that can meet the demands of research and industry alike.

This paper is composed of five sections. A critical literature review on PEMWE and alkaline modelling is presented in Section 2. A description of the modelling library is given in Section 3. The verification of the tool for parameterizing the polarisation curve of a water electrolyzer is presented in

Section 4. Finally, Section 5 concludes the study by summarizing key aspects of the work.

Theory

The principle underlying water electrolysis is that electrochemical reactions break water molecules to form hydrogen at the cathode and oxygen at the anode. The overall reaction is the same for all water electrolysis technologies:

$$H_2O(l) \rightleftharpoons \frac{1}{2}O_2(g) + H_2(g), \tag{1}$$

but the different technologies differ in their half-cell electrode reactions. For PEM electrolysis, the half reactions are [20]:

$$2H^+(aq) + 2e^- \rightleftharpoons H_2(g), \text{ and} \tag{2}$$

$$H_2O(l) \rightleftharpoons \frac{1}{2}O_2(g) + 2H^+(aq) + 2e^- \tag{3}$$

for the cathode and the anode, respectively. The corresponding half reactions for AWE, on the other hand, are [20]:

$$2H_2O(l) + 2\ e^- \rightleftharpoons H_2(g) + 2\ OH^-(aq), \quad \text{and} \tag{4}$$

$$2OH^-(aq) \rightleftharpoons \frac{1}{2}\ O_2(g) + H_2O(l) + 2e^-. \tag{5}$$

The production rate of hydrogen molecules in water electrolysis, $\dot{n}_{H_2}$, is directly proportional to the current density j and current efficiency η_F, also known as Faraday efficiency. The relationship is portrayed in Faraday's law of electrolysis:

$$\dot{n}_{H_2} = \eta_F \frac{jA}{n_e F}, \tag{6}$$

where A is the active surface area, n_e is the number of electrons involved in the creation of one molecule of hydrogen, which in the case of water electrolysis is two, and F is the Faraday constant. Based on Eq. (1) the current efficiency for an ideal system can be assumed to equal unity, as there are no obvious side reactions that consume current in the process. In real-world water electrolyzer systems, however, gas crossover phenomena and stray currents reduce the current efficiency.

Voltage analysis of the system is required when assessing the total energy efficiency of the electrolysis process. In electrolytic hydrogen production, the cell voltage U_{cell} is the sum of the open circuit voltage U_{ocv}, also known as the Nernst potential or reversible potential, and additional overpotentials:

$$U_{cell} = U_{ocv} + U_{ohm} + U_{act} + U_{con}, \tag{7}$$

where U_{ohm} is the overpotential caused by ohmic losses, U_{act} the activation overpotential and U_{con} the concentration overpotential resulting from mass transport phenomena [21]. Building a comprehensive modelling tool requires implementation and understanding of each voltage component.

Open circuit voltage

The open circuit voltage (OCV) U_{ocv} is the lowest potential level that facilitates the electrolysis process. The OCV describes the thermodynamics of the electrochemical reactions [20] and is related to the Gibbs free energy change ΔG of the reaction:

$$U_{ocv} = \frac{\Delta G}{n_e F}. \tag{8}$$

The Gibbs free energy change is dependent on the environment, specifically, on the temperature T and activity of the reacting species a, which is why the OCV is often presented with the Nernst equation:

$$U_{ocv} = U^\circ + \frac{\mathcal{R}T}{n_e F} \ln \frac{\prod_k a_{O_k}^{\nu_{O_k}}}{\prod_l a_{R_l}^{\nu_{R_l}}}. \tag{9}$$

Eq. (9) is valid for a generic electrochemical reaction in a reversible system:

$$\sum_k \nu_{O_k} O_k + n_e e^- \rightleftharpoons \sum_l \nu_{R_l} R_l, \tag{10}$$

where O represents the oxidized species, R is the reduced species in the reaction, ν_X is the stoichiometric coefficient, and a_X the activity of the specific species X. U° in Eq. (9) is a temperature-dependent reference voltage for the reaction in standard pressure and reagent concentrations, whereas non-standard reaction conditions are accounted for by the rest of the equation.

The open circuit voltage for a combined cell can be calculated from the potentials of the anodic and cathodic half reactions:

$$U_{ocv} = U_{ocv,a} - U_{ocv,c}. \tag{11}$$

Finding the OCV for both half reactions and combining them according to Eq. (11) will result in a single open circuit voltage for water electrolysis. For PEMWE, the Nernst equation for anodic (Eq. (3)) and cathodic (Eq. (2)) half reactions are:

$$U_{ocv,a} = U_a^\circ + fT \ln \frac{a_{O_2}^{1/2} a_{H^+}^2}{a_{H_2O}}, \quad \text{and} \tag{12}$$

$$U_{ocv,c} = U_c^\circ + fT \ln \frac{a_{H^+}^2}{a_{H_2}}, \tag{13}$$

respectively. To simplify the equations, the following shortened symboling is defined and used from Eq. (12) onward:

$$f = \frac{\mathcal{R}}{n_e F}. \tag{14}$$

In PEMWE, the reaction at the cathode is a hydrogen evolution reaction (HER), Eq. (2), whose standard potential $U_c^\circ = 0$ by definition. Therefore, the unified reversible potential of water electrolysis, defined as $U = U_a^\circ - U_c^\circ$, can be simplified to $U = U_a^\circ$ for PEMWE [22]. Applying Eq. (12) and Eq. (13) to Eq. (11), we find the Nernst equation for the total electrolysis reaction to be:

$$U_{ocv} = U^\circ + fT \ln \frac{a_{H_2} a_{O_2}^{1/2}}{a_{H_2O}}. \tag{15}$$

Exactly the same result can be derived for AWE, although the anodic and cathodic half reactions differ. Difference in the half reactions leads to different standard potentials for $U_a^\circ U_a^\circ$

Table 1 – Standard potentials of the water electrolysis half-cell reactions for both PEMWE and AWE [23].

	PEMWE		AWE	
Cathode (U_c°)	0 V	Eq. (2)	−0.8277 V	Eq. (4)
Anode (U_a°)	1.229 V	Eq. (3)	0.401 V	Eq. (5)

and U_c° (see Table 1). However, the unified reversible potential U° is equal regardless of the technology.

Reversible potential

The standard reversible potential U° for the electrolytic water splitting reaction can be determined using common, experimental formulae. LeRoy et al. [24] derived a widely used approximation, Eq. (16), from experimentally determined temperature-dependent reaction enthalpy using the Gibbs–Helmholtz equation. Linear approximations have also been used, for example, Schalenbach et al. [22] applied an experimental linear approximation, borrowed from fuel cell research [25] to electrolyzers. Schalenbach [26] later proposed an updated equation Eq. (18) which, nevertheless, was still based on linear approximation. Hammoudi et al. [10] proposed a polynomial approximation derived from the Gibbs–Helmholtz thermodynamic relation between the enthalpy and the Gibbs free energy. Equations from Dale et al. [13] and from da Costa Lopes [27] are also included in the tool.

$$U^\circ = 1.5184 - 1.5421\times10^{-3}T + 9.523\times10^{-5}T\ln T + 9.84\times10^{-8}T^2\,(\mathrm{V}) \tag{16}$$

$$U^\circ = 1.229\,\mathrm{V} - (0.000846\,\mathrm{VK^{-1}})(T - 298.15) \tag{17}$$

$$U^\circ = \frac{1}{n_e F}\left[\left(-159.6\ \mathrm{J\ mol^{-1}\ K^1}\right)T + 2.8472\times10^5\ \mathrm{J\ mol^{-1}}\right] \tag{18}$$

$$U^\circ = 1.50342\mathrm{V} - (9.956\times10^{-4}\ \mathrm{VK^{-1}})T + (2.5\times10^{-7}\ \mathrm{VK^{-2}})T^2 \tag{19}$$

$$U^\circ = 1.5241 - 1.2261\times10^{-3}T + 1.1858\times10^{-5}T\ln T + 5.6692\times10^{-7}T^2\,(\mathrm{V}) \tag{20}$$

$$U^\circ = 1.449\mathrm{V} - (6.139\times10^{-4}\ \mathrm{VK^{-1}})T - (4.592\times10^{-7}\ \mathrm{VK^{-1}})T^2 + (1.46\times10^{-10}\ \mathrm{VK^{-1}})T^3 \tag{21}$$

The results of equations (16–21) differ only slightly in the usual operating temperature range of PEMWE, as shown in Fig. 1, making them all equally valid.

Species activity

The activity a_X for an ideal gas can be expressed as the ratio of its partial pressure p_X to a standard, reference pressure $p^\circ = 1$ bar. The reference pressure is the pressure at which the standard reversible potential U° is defined [28]:

$$a_X = \frac{p_X}{p^\circ}. \tag{22}$$

Activity a_{H_2O} for pure liquid water at the electrodes in PEM water electrolysis can be expressed as unity [28]. Water activity in the electrolyte solution for AWE, on the other hand, can be calculated as the fraction of saturated water vapor pressure in contact with the electrolyte $p_{sv,el}(T, m)$ compared to the saturated vapor pressure in pure water $p_{sv}(T)$:

$$a_{H_2O,el} = \frac{p_{sv,el}(T,m)}{p_{sv}(T)}. \tag{23}$$

With the assumptions that the gas mixtures within the system are ideal, that there is no gas crossover, and that the saturated water vapor pressure is only a function of temperature, the partial pressures of the gasses can be calculated using Dalton's law from the measured pressure p_a for the anode and p_c for the cathode by subtracting the water vapor pressure [29]:

$$p_{H_2} = p_c - p_{sv}(T), \tag{24}$$

$$p_{O_2} = p_a - p_{sv}(T). \tag{25}$$

In AWE, the gases on the two electrodes can be assumed to be at equal pressure p for which reason the following applies:

$$p_{H_2} = p_{O_2} = p - p_{sv,el}(T,m). \tag{26}$$

Now Eq. (15) can be modified to the forms:

$$U_{ocv} = U^\circ + fT\ln\frac{(p_c - p_{sv}(T))(p_a - p_{sv}(T))^{1/2}}{p^{\circ 3/2}} \quad \text{for PEMWE, and} \tag{27}$$

$$U_{ocv} = U^\circ + fT\ln\frac{(p - p_{sv,\,el}(T,m))^{3/2}p_{sv}(T)}{p^{\circ 3/2}p_{sv,\,el}(T,m)} \quad \text{for AWE.} \tag{28}$$

The saturated water vapor pressure for pure water can be calculated from the Antoine equation:

$$\log_{10}p_{sv}(T) = A - \frac{B}{T+C}, \tag{29}$$

where parameters A, B and C are given for different temperature ranges in Table 2. Another option is to use an experimental equation obtained by J. Balej [31]:

$$\log_{10}p_{sv}(T) = 35.4462 - \frac{3343.93}{T} - 10.9\ \log_{10}T + 4.1645\times10^{-3}T. \tag{30}$$

The result from these two methods are nearly indistinguishable within the temperature range of 0 °C–100 °C. Alkaline electrolyte vapor pressure $p_{sv,el}(T, m)$, is determined from the vapor pressure of pure water $p_{sv}(T)$ by [31]:

$$p_{sv,el}(T,m) = 10^a p_{sv}(T)^b. \tag{31}$$

Parameters a and b depend on the electrolyte type and its molality m:

$$a = \begin{cases} -0.01508\,m - 1.6788 \times 10^{-3}\,m^2 + 2.25887 \times 10^{-5}\,m^3, & \text{for KOH} \\ -0.010986\,m - 1.461 \times 10^{-3}\,m^2 + 2.03528 \times 10^{-5}\,m^3, & \text{for KOH} \end{cases} \quad (32)$$

$$b = \begin{cases} 1 - 1.2062 \times 10^{-3}\,m + 5.6024 \times 10^{-4}\,m^2 - 7.8228 \times 10^{-6}\,m^3, & \text{for KOH} \\ 1 - 1.34141 \times 10^{-3}\,m + 7.07241 \times 10^{-4}\,m^2 - 9.5362 \times 10^{-6}\,m^3, & \text{for NaOH.} \end{cases} \quad (33)$$

The unit of pressure has to be bar for these given parameters to work.

Activation overpotential

Activation overpotential accounts for the energy losses due to charge transfer kinetics in water electrolysis. It represents the voltage needed to overcome the reaction energy barriers to initiate a sufficiently high reaction rate in the wanted direction. The activation overpotential at each electrode-electrolyte interface is implicitly defined by the Butler–Volmer (B–V) equation, with a common assumption that the rate-determining step in the reaction is a one-step, single-electron transfer process [32]:

$$j = j_{0,c}\left[\exp\left(\frac{\alpha_c}{fT}U_{act,c}\right) - \exp\left(-\frac{(1-\alpha_c)}{fT}U_{act,c}\right)\right], \quad (34)$$

where $j_{0,c}$ is the exchange current density and $\alpha_c \in [0, 1]$ the so-called electron transfer coefficient [33]. The subscript c is used here to signify that the equation is for the half reaction at the cathode, but the same equation is used for the reaction at the anode.

In Eq. (34), the forward reaction is accounted for by the first exponential term and the backward reaction by the second exponential term. Exchange current density j_0 is dependent on the properties of the catalyst layer and temperature with an Arrhenius-type relation [8,32,34–36], and $j_{0,c}$ should therefore, in practice, be experimentally defined for each setup. Electron transfer coefficient α is reaction and temperature-dependent and describes the balance between the forward and backward rates of the reaction. For simplicity, α is commonly assumed to be 0.5, but the validity of this assumption, especially for the oxygen evolution reaction at the anode, is questionable [29]. Therefore, other values for α are also used in the literature to match experimental data. The effect of variation of α and j_0 on the activation overpotential is depicted in Fig. 2.

Since the full B–V equation must be solved implicitly for the activation overpotential, a variety of explicit approximations have been utilized in the literature, namely the Tafel equation and hyperbolic sine approximation. The presented approximations come with their own range of applicability, which has to be understood to minimize modelling inaccuracies.

Tafel equation

A common approximation of the Butler–Volmer equation is the Tafel equation. By assuming operation far from kinetic equilibrium, which means that U_{act} in Eq. (34) is either much

Table 2 – Parameters for Antoine equation in four temperature ranges [30].

Temperature range [K]	A	B	C
273 … 304	5.40221	1836.675	−31.737
304 … 334	5.20389	1733.926	−39.485
334 … 363	5.0768	1659.793	−45.854
363 … 374	5.08354	1663.125	−45.622

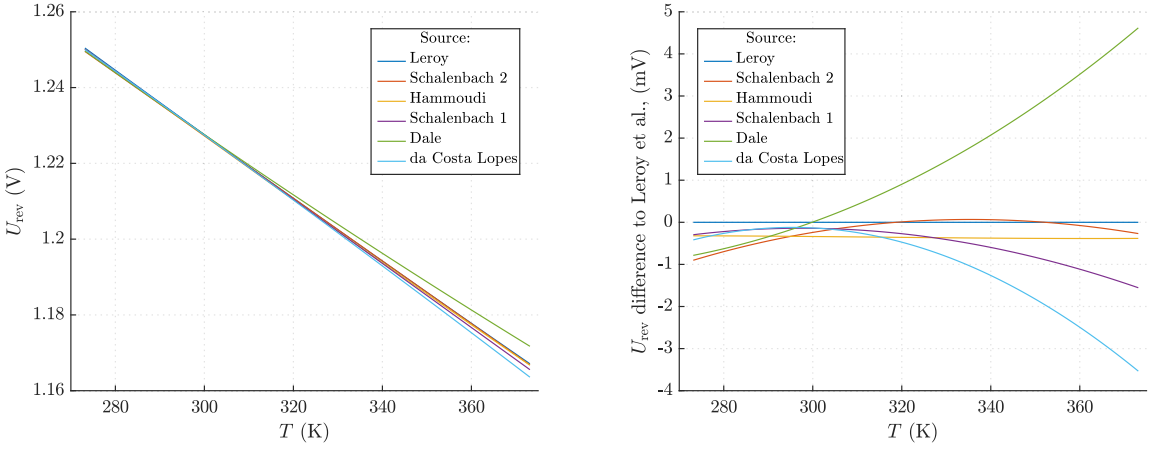

(a) Definite values (b) Absolute differences to Leroy et al. [24]

Fig. 1 – Comparison between different approximations of reversible potential as a function of temperature. The equations for each approximation are as follows: Leroy Eq. (16), Schalenbach 1 Eq. (17), Schalenbach 2 Eq. (18), Hammoudi Eq. (19), Dale Eq. (20), and Da Costa Eq. (21).

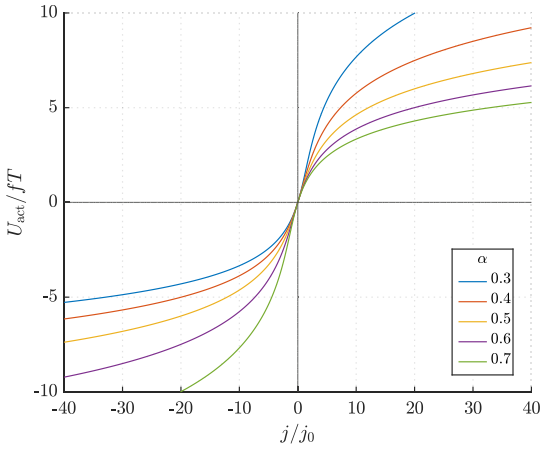

(a) Butler–Volmer equation for variable values of α.

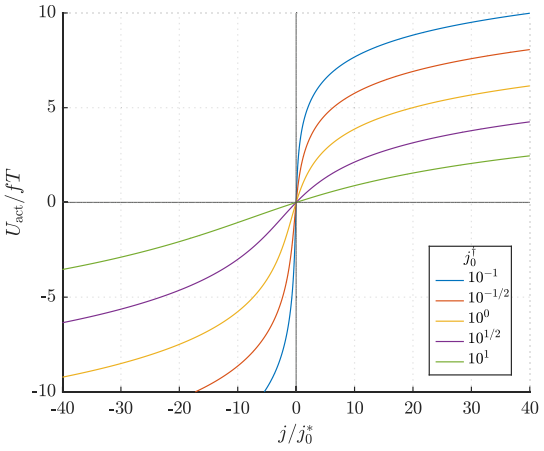

(b) Butler–Volmer equation for variable values of j_0 with $\alpha = 0.6$ picked to illustrate a case where B–V equation doesn't result in odd symmetry in the resulting curve.

Fig. 2 – Behaviour of the Butler–Volmer equation as a function of parameters (a) α and (b) j_0. To maintain non-dimensionality of the x-axis in the figure (b), the effective change in the value of j_0 is separated to a multiplier $j_0^\dagger$ used as the variable ($j_0 = j_0^* j_0^\dagger$).

greater or much smaller than 0, one of the exponent terms can be assumed to be insignificant. For example, if positive voltage and current signs are defined for the electrolytic reaction and $U_{act} \gg 0$, Eq. (34) for the cathode can be simplified to the Tafel equation:

$$j = j_{0,c}\exp\left(\frac{\alpha_c}{fT}U_{act,c}\right) \Leftrightarrow U_{act,c} = a_c \ln\frac{j}{j_{0,c}}, \tag{35}$$

with a parameter called the Tafel slope, which is defined as $a_c = fT/\alpha_c$. The same equation is valid for the anode. As the Tafel equation requires an assumption of high enough activation overpotential, it can be considered valid only when $j/j_0 > 4$ [32]. Comparison between the Butler–Volmer equation and the Tafel equation is presented in Fig. 3.

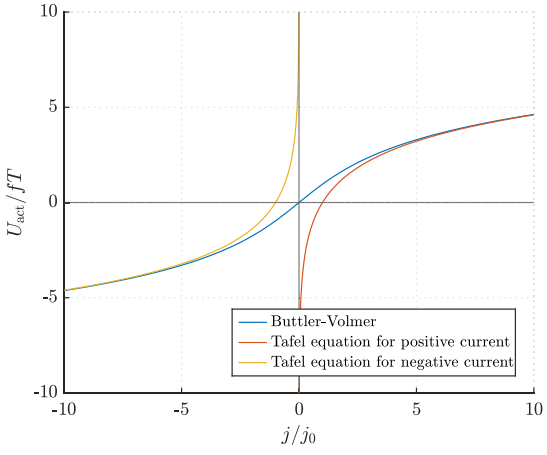

Fig. 3 – Tafel equation compared to Butler–Volmer equation with $\alpha = 0.5$.

Hyperbolic sine approximation

Another approximation approach found in the literature [8,37,38] to modify the Butler–Volmer equation into a closed form for U_{act} is to use the definition of the hyperbolic sine:

$$\sinh x = \frac{\exp(x) - \exp(-x)}{2}. \tag{36}$$

Approximation is done similarly for both the anode and cathode, but here we again use the cathode as an example.

The approximation is based on the assumption that $\alpha_c = 1/2$, which has been found to be accurate at least for hydrogen evolution and the hydrogen oxidation reaction pair [39] but not so for oxygen evolution and oxygen reduction reactions [29]. With this assumption, the Butler–Volmer equation Eq. (34) can be modified to the form:

$$j = 2j_{0,c}\sinh\left(\frac{1}{2fT}U_{act,c}\right), \tag{37}$$

using the definition in Eq. (36). The activation overpotential is now solvable:

$$U_{act,c} = 2fT\, arsinh\frac{j}{2j_{0,c}}. \tag{38}$$

Despite the fact that the hyperbolic sine approximation is derived only for the case $\alpha_c = 1/2$, some authors use a variable α_c together with the hyperbolic sine approximation [38,40]:

$$U_{act,c} = \frac{fT}{\alpha_c} arsinh\frac{j}{2j_{0,c}}. \tag{39}$$

Visual analysis of the validity of this approximation, shown in Fig. 4 illustrates that when the value of α differs from 1/2 the approximation diverges from the Butler–Volmer

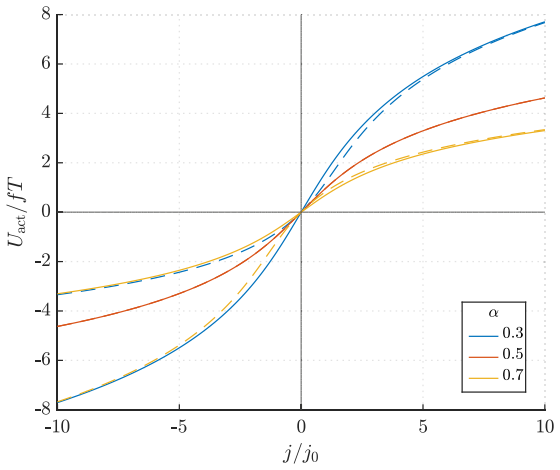

Fig. 4 – Comparison between the hyperbolic sine approximation and the Butler–Volmer equation for three values of α. The Butler–Volmer equation is shown with a dashed line.

equation, especially at low current densities. The difference between the B–V equation and the hyperbolic sine approximation is, however, much less than between the B–V equation and the Tafel approximation, Fig. 3, making the hyperbolic sine approximation more suitable for lower current densities. If the current is reversed, the hyperbolic sine approximation diverges drastically from the B–V equation. The hyperbolic sine approximation is, therefore, valid only for one-directional reactions. In electrolysis research it is in any case preferable to keep the reactions in one direction only with high enough currents as this minimizes the safety issues caused by gas crossover phenomena, which enables the use of either of the approximations presented.

Combined electrodes and the accuracy of the Butler–Volmer equation

Thus far, the activation phenomena have been presented for individual electrodes only. However, the same approximative equations are often used for the combined activation overpotentials of the anode and the cathode [38,41–43]:

$$U_{act} = U_{act,c} + U_{act,a}. \tag{40}$$

Using Eqs. (35), (38) and (39) for the combined activation overpotential voltage leads to equations:

$$U_{act} = a \ln \frac{j}{j_0}, \tag{41}$$

$$U_{act} = 2fT\, arsinh \frac{j}{2j_0}, \text{and} \tag{42}$$

$$U_{act} = \frac{fT}{\alpha} arsinh \frac{j}{2j_0}, \tag{43}$$

respectively. When a fit is made to experimental results for which the electrode overpotentials have not been measured separately, only single, combined values for α and j_0 can be obtained. As discussed by Noren and Hoffman [32], however, the approach of combining the electrode overpotentials, and modelling them with single parameter values for α and j_0 will lead to a loss of physical meaning of the fit parameters. The predictive capability of such models is, therefore, questionable outside the exact systems that they were measured from.

The validity of the B–V equation for modelling water electrolysis has, furthermore been questioned from a microkinetic point of view. Shinagawa et al. [44] reason that as the rate-determining step may differ between the forward and backward reactions, the kinetics of the reaction cannot simply be presented by the B–V equation. However, as the equation has been used with adequate accuracy to describe the experimental U–I behaviour of electrolytic cells, it is widely used in modelling the kinetics in the macro regime. Using the B–V equation regardless of its possible unsuitability for water electrolysis modelling may lead to further loss of physical meaning for the parameters.

Ohmic overpotential

The ohmic overpotential can be calculated based on Ohm's law:

$$U_{ohm} = rj. \tag{44}$$

The total area-specific resistance of the cell r consists of resistance over multiple serially connected regions, from which the electronic and ionic area-specific resistances, marked with r_e and r_i, respectively, are simple to separate:

$$U_{ohm} = (r_e + r_i)j, \tag{45}$$

Both r_e and r_i can be generally calculated by integrating material resistivity ρ over the current conduction path:

$$r = \int_0^l \rho(x)\, dx. \tag{46}$$

Calculating the integral in Eq. (46) for the electronic area specific resistance r_e is often challenging. The current path is comprised of multiple separate materials in series, such as bipolar plates and porous transport layers, and their interfaces, whose properties can vary significantly having a measurable impact on their resistivity. Thus, the most convenient way is to determine the electronic resistance from polarisation curve measurements as a fit parameter.

The ionic area specific resistance, r_i, is generally more significant than that of the electronic conductors (r_e) [45]. The ionic conduction path within the electrolyzer cell is shorter and more uniform than the electronic path, and thus the ionic area-specific resistance is often simplified by assuming constant resistivity. This assumption leads to a simple solution for Eq. (46) [8]:

$$r_i = \frac{\delta}{\sigma}, \tag{47}$$

where the conduction path is depicted by the electrolyte layer thickness δ, and the conductivity of the material σ through which the ions traverse, being the reciprocal of resistivity ρ, is often used instead of resistivity.

Marangio et al. [40] proposed a more complete equation for the ionic resistance across a PEM electrolyte membrane, which is derived from an equation for the electric potential gradient across the membrane by Bernardi et al. [46]. However, Marangio et al. [40] showed, that the decrease in accuracy when using the simplified equation Eq. (47) is very small in current range of 0 A–2 A, while requiring fewer parameters.

For PEMWE the distance δ is represented by the membrane thickness, and its conductivity σ can be experimentally determined or calculated from an experimentally determined equation. One experimental equation is proposed by Springer et al. [47], where the membrane conductivity can be determined based on the temperature and water content of the membrane:

$$\sigma = 0.005139\,\lambda - 0.0326\,\exp\left[1268\left(\frac{1}{303}-\frac{1}{T}\right)\right]. \tag{48}$$

Here, λ is the water content (ratio of water molecules to the charge (SO_3^-) sites in the Nafion® membrane) and T is temperature in kelvin.

In AWE, σ is determined from fits done to experiment data. For KOH, Gilliam et al. [48] presented the following equation applicable in the 0 °C–100 °C temperature range, where the conductivity is presented as a function of molarity M and temperature T:

$$\begin{aligned}\sigma = & -2.041\,M - 0.0028\,M^2 + 0.005332\,MT + 207.2\,(M/T)\\ & +0.001043\,M^3 - 3\times10^{-7}\,M^2T^2.\end{aligned} \tag{49}$$

A second widely used conductivity equation for KOH was presented by See et al. [49] for the −15 °C to 100 °C temperature range in which conductivity is a function of mass fraction w and temperature T:

$$\begin{aligned}\sigma = & \ 27.9844803\,w - 0.009241294\,T - 1.49660371\times10^{-4}\,T^2\\ & -0.0905209551\,Tw + 2.59087043\times10^{-4}\,(T^2w^{0.1765})\\ & +6.96648518\times10^{-4}\,(T/w) - 2898.15658\,(w/T).\end{aligned} \tag{50}$$

For NaOH LeBideau et al. [50] developed a fit based on data from Zaytsev et al. [51] using the least square method:

$$\begin{aligned}\sigma = & -4.57 + 1.02\,T + 3.20\times10^3\,w^3 - 2.99\times10^3\,w^2 + 7.84\\ & \times10^2\,w.\end{aligned} \tag{51}$$

Their fit has a quite small temperature range of 25 °C–50 °C limiting its use cases.

Concentration overpotential

The concentration overpotential results from the mass transport limitations at the electrodes, and it is significant mostly at high cell currents. For AWE, high enough current density has a distinguishable effect on the water concentration at the electrode surfaces compared to the bulk electrolyte, decreasing the water concentration at the cathode and increasing it at the anode, according to Eqs. (4) and (5), respectively. Dissimilar changes in the electrolyte concentrations between the electrodes, and locally rising oxygen and hydrogen partial pressures have an effect on the respective species activity, which in turn increases the open circuit voltage of the half reactions.

For PEMWE, the reaction takes place at the membrane-electrode interface, and all the reactant and product mass flows have to be transported through the porous electrode. There is a flow resistance for the mass flow going through the electrode which increases with increasing flow. Flow through the porous electrode is a diffusion phenomenon which can be described by Fick's law as only two-component mixtures are present in the water electrolysis process. Product transport limitations cause most of the overpotential as H_2 and O_2 have to be removed as fast as they are produced or their concentration increases, which slows down the reaction kinetics [40]. In addition, the creation of oxygen bubbles on the anode reduces the active surface area available for the reaction.

These mass transport issues are represented in the concentration overpotential U_{con} which can be estimated using the Nernst equation formulized with the reagent concentrations:

$$U_{con} = fT\ln\frac{C_{O_2}^{1/2}C_{H_2}}{C_{O_2,0}^{1/2}C_{H_2,0}}, \tag{52}$$

where $C_{X,0}$ represents the concentration of reagent X at the membrane-electrode interface in a reference working condition and C_X is the concentration after mass transfer has occurred [40].

For PEMWE an alternative way to model the concentration overpotential is to add a current limiting term to the anodic activation overpotential [9]:

$$U_{act,\,a} = \frac{fT}{\alpha_a}\ln\frac{\frac{j_a}{j_{0,a}}}{1-\frac{j_a}{j_{L,a}}}, \tag{53}$$

where α_a is the anode side electron transfer coefficient, j_a is the anode side current density, $j_{0,a}$ is the exchange current density, and $j_{L,a}$ is the current limiting term. The current limiting term is added to the anode side as the oxygen bubbles would block the electrode surface at high current densities. For PEMWE the cathode reaction is not dependent on liquid water as a reagent at the reaction site, which implies that bubble formation is not an issue there.

The concentration overpotential can be separated from the activation potential to its own term:

$$U_{con} = -\frac{fT}{\alpha_a}\ln\left(1-\frac{j}{j_{L,a}}\right). \tag{54}$$

Alternatively, the same equation has been used by some authors without the electron transfer coefficient [41]:

$$U_{con} = -fT\ln\left(1-\frac{j}{j_L}\right). \tag{55}$$

The form of Eq. (55) is more useful with combined-electrode models where the separate anodic electron transfer coefficient α_a is unknown.

Consideration of the constant reversible potential offset

The theory presented from Section 2.1 to Section 2.4 provides equations for calculating the polarisation curve with four parameters that have to be fitted from an experimental polarisation curve: electron transfer coefficient α, exchange

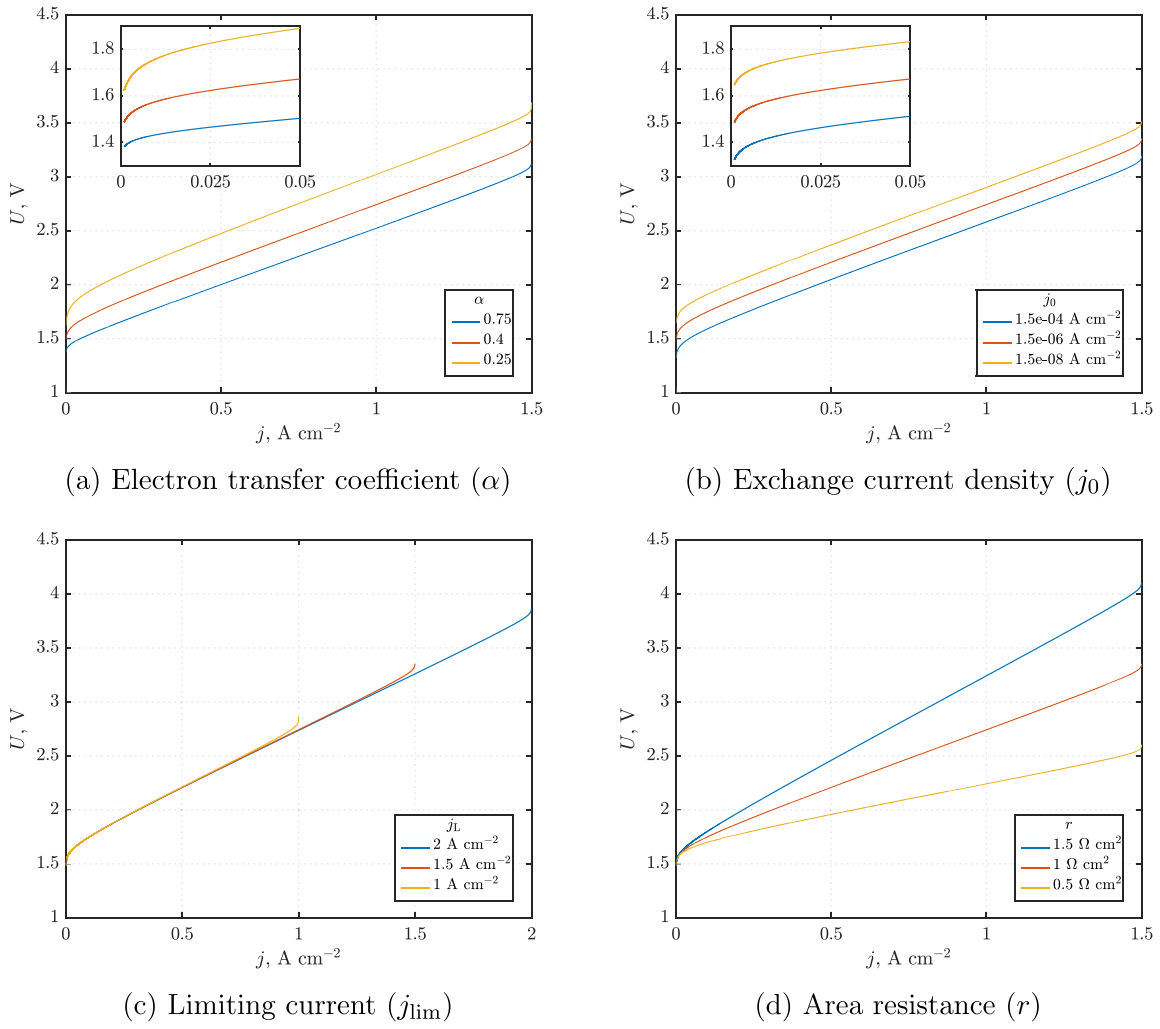

(a) Electron transfer coefficient (α)

(b) Exchange current density (j_0)

(c) Limiting current (j_{lim})

(d) Area resistance (r)

Fig. 5 – Effect of different fitting parameters on the resulting polarisation curve. The images for α and j_0 include a magnified view of the low current densities. In each of the figures the parameter values that are not variable are $\alpha = 0.4$, $j_0 = 1.5 \times 10^{-6}$ A cm^{-2}, $j_L = 1.5$ A cm^{-2}, and $r = 1\ \Omega$ cm^2.

current density j_0, area specific resistance r, and limiting current density j_L. These four parameters all have a distinct effect on the polarisation curve, as can be seen from Fig. 5, which enables the use of a curve fit for finding their values. A fifth fitting parameter sometimes used in the literature is a voltage offset, implemented as a variable standard reversible potential U° [38]. This is a tempting approach, as such a parameter can indicate whether unwanted electrochemical reactions are occurring inside the cell. However, if the Butler-Volmer equation, Eq. (34), is rearranged into the following form:

$$\frac{j}{j_0^*} = \exp\left(\frac{\alpha}{fT}U_{\text{act}} + \ln j_0^\dagger\right) - \exp\left(\frac{\alpha - 1}{fT}U_{\text{act}} + \ln j_0^\dagger\right), \tag{56}$$

by defining $j_0 = j_0^* j_0^\dagger$ where j_0^* represents the original exchange current density, and $j_0^\dagger$ stands for a multiplier change in its value, it can be noted that change in the exchange current density j_0 affects the activation overpotential in a similar way as if there was an offset of voltage. The described effect is most pronounced if $\alpha = 0.5$ or if the operational point is far enough from equilibrium to reduce one of the exponent terms.

Fig. 5b shows clearly the resemblance between the effects on the polarisation curve caused by changing the exchange current density and adding a potential offset. The same effect can also be noted in Fig. 2b. Including a potential offset as an additional fitting parameter is, therefore, prone to degrade the fitting performance of the exchange current density. In this study, implementation of the potential offset was, thus, abandoned because of the observed overlapping effects.

Simulation software methodology

A water electrolyzer modelling tool was developed with capabilities to model and parameterize measured polarisation curves for PEMWE and AWE. All the potentials presented in Section 2 are modelled in the simulation tooling. Multiple

different models for overpotentials and for reversible potential are available, which can be selected depending on the measurement data at hand, while also taking into account other limitations and needs. Currently available models are listed in Table 3. Expanding the modelling library with new models is easy, and the tool has been designed to be very flexible, allowing users to add models of interest in to the tooling with minimal work. A simplified flow chart of the modelling tool is shown in Fig. 6.

Each voltage component is separated into its own module, which can then be combined as the user requires. The combined voltage equation can then be used in either the parametrization or modelling part of the tool. To perform the parameter fitting, the user has to provide a set of measured voltage and current value pairs and also common variables such as temperature and pressure, and electrolyte molality in the case of AWE, which have been kept constant for the system. Polarisation curve parameters, like the resistance of the cells, are usually difficult to measure directly from the system or are difficult to solve, like the electron transfer coefficient. Because of the difficulty of obtaining the parameters with other methods, curve fitting is generally used. Once the parameters have been obtained, they can be used in the modelling part of the tool to calculate the voltage of the water electrolyzer at different currents.

Fitting

In the modelling tool, fitting is implemented using standard fitting functions found in MATLAB. Fitting is used because

Table 3 – Models available in the tooling for PEMWE where the first model of each category is the default model.

Term	Model number	Electrolyzer type	Reference	Equation
Standard reversible potential	1		[12]	(18)
	2		[24]	(16)
	3		[13]	(20)
	4		[10]	(19)
	5		[25]	(17)
	6		[27]	(21)
Pressure correction for OCV	–	Alkaline	–	(28)
	–	PEM	–	(27)
Activation overpotential	1		–	(43)
	2		–	(42)
	3		–	(41)
Ohmic overpotential	1		–	(44)
	2		[8]	(45)
Conductivity	2.1	Alkaline	[48]	(49)
	2.2	Alkaline	[49]	(50)
	2.3	PEM	[47]	(48)
Concentration overpotential	1		[41]	(55)
	2		[40]	(52)

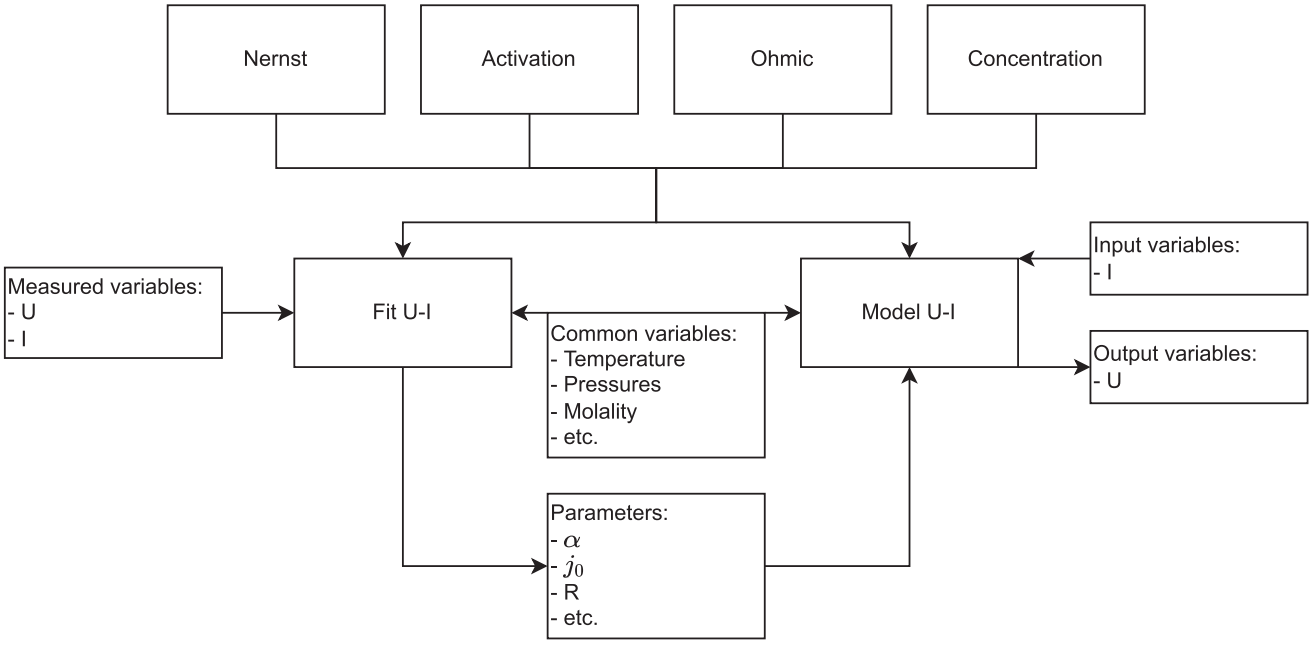

Fig. 6 – Simplified flow chart of the modelling tool.

some parameters that are necessary for the models such as the resistance and electron transfer coefficient are difficult to obtain by means of measurements or calculations. For such parameters, curve fitting presents a good method to find suitable values that enable modelling of the system.

The tool includes an abstraction layer for standard MATLAB fitting functions to simplify the process of parameterizing water electrolyzer polarisation curves. The end user has to only provide the measured voltage, current, and common parameters such as temperature and pressure measured from the system, after which the fitting function can be called to do the curve fitting for the rest of the parameters. Error bounds are automatically calculated for each fitted parameter.

Two common fitting methods were implemented in the modelling tool, Non-linear Least Squares Error regression (NLLSE) and Particle Swarm Optimisation (PSO) based minimization. The minimization is performed on the sum of squared residuals of the fitted curve. NLLSE is very commonly used for estimation calculations, as it can be used with a wide variety of functions. PSO, on the other hand, is a method which iteratively tries to minimize the given objective function, by having a population of candidate solutions which are moved in the given search space towards the optimal solution [52]. The starting position of the particles is completely random, which can result in some random variation in the fitting result. In initial tests, NLLSE was noticed to produce bad fitting results for certain data sets, which prompted the addition of PSO as an option to reduce the number of cases where no good fit can be found. Comparing the methods highlights the strengths and weaknesses of both approaches. For easy comparison of results, error bounds are automatically calculated. In the case of NLLSE MATLAB Curve Fitting Toolbox is used, which calculates the error bounds based on Jacobian of the fitted values. For PSO the error bounds are calculated using the Markov Chain Monte Carlo method. The Markov Chain Monte Carlo error bounds are calculated with a library created by M. Laine [53].

Water electrolyzer parametrization

Measurement data for validation and parametrization were obtained from a PEMWE test system located in the Forschungszentrum Jülich, Germany and from an AWE system at LUT University, Finland.

The membrane electrode assembly for the PEMWE was fabricated in Jülich using a similar decal process to that presented by Stähler et al. [54]. A FuelCon electrolyzer test rig (C1000-LT) was used for the measurements. Simplified P&I diagram of the test setup is presented in Fig. 7. The voltage was measured with a GN840B sensor from HBM and the current with a DC current transducer Flux CT600 from CAENels. Specifications of the PEMWE are listed in Table 4.

AWE measurements were conducted using an electrolyzer stack made by Light Bridge Inc. Further specifications are given in Table 5. For the electrolyte NaOH was used as that was readily available. Because the test results were used only to verify the fitting performance of the tool, the efficiency of the water electrolyzer was not critical. Simplified P&I diagram of the AWE test setup is shown in Fig. 8. Voltage and current

Table 4 – PEMWE system specifications.

Manufacturer:	Forschungszentrum Jülich, IEK-14
Membrane:	Nafion 117
Number cells:	1
Nominal voltage:	2 V
Nominal current:	36 A
Nominal power:	72 W
Active area	17.64 cm^2
Electrode cathode:	Pt, 0.39 mg cm^{-2}
Electrode anode:	Ir, 2.19 mg cm^{-2}
Porous transport layer (PTL), cathode:	Toray paper
PTL, anode	Sintered titanium, coated with iridium

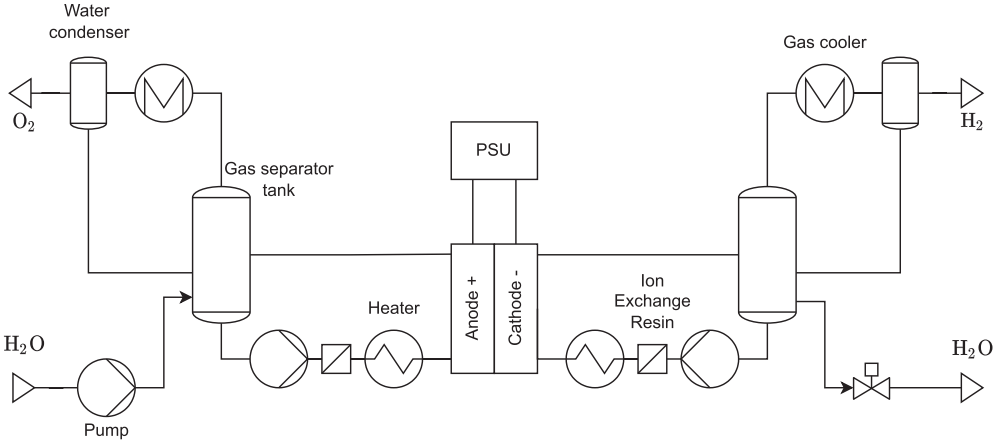

Fig. 7 – Simplified P&I diagram of the PEM test setup. Diagram is modified from the one presented in Koponen et al. [12], where the same system configuration was previously used.

Table 5 – AWE system specifications.

Manufacturer:	Light Bridge
Electrolyte:	20 wt% NaOH
Number cells:	10
Nominal voltage:	20 V
Nominal current:	17.5 A
Nominal power:	350 W
Active area:	152 cm^2
Separator:	Porous polymer
Electrodes:	Nickel based compound

were measured with a Hioki PW6001 power analyser using a CT6863-05 current probe.

Polarisation curves were measured for both electrolyzers and environmental variables such as temperature were noted. This approach allows accurate modelling of both systems using the modelling tool developed. Both data sets include measurement data starting from low current densities, where activation overpotentials are dominant, and from the linear operation zone, which is dominated by the ohmic overpotentials. In both the PEMWE and the AWE, the current densities were not high enough for concentration overpotentials to have a significant effect.

Measurement conditions were controlled for temperature change. The PEMWE was kept at constant 75 °C, whereas the measurements for the alkaline system were conducted at both 30 °C and 60 °C. The alkaline system also had continuous temperature measurement, which provided the temperature data at each current step. Both systems were operated at ambient pressure.

In the validation tests measured current and voltage were loaded into the modelling tool, which was set up to use the default equations presented in Table 3. For the alkaline system, the measured temperature data was also used to improve fitting accuracy. Both NLLSE and PSO were tested to see the performance difference between the implementations.

Simulations were conducted to verify that the tooling works as expected and to explore the effects of different quality data on the fitting results. Results for fitting are presented in Fig. 9 for the PEMWE and in Fig. 10 for the AWE.

For the PEMWE system, the measured current-voltage data could be fitted almost perfectly with both the NLLSE and the PSO method. Fitting results are shown in Fig. 9 and the fitted parameters are listed in Table 6. As can be noted from the very high R^2 value, the tool was able to produce very accurate fits in both cases. Values for most parameters are also close to each other; however, the results are not in full agreement with each other within the confidence bounds. Limiting current density was omitted from the modelling, as the measurement data did not contain data for high enough current densities where the phenomena could be seen.

The measurement data from the AWE system presented more of a challenge, especially at low temperatures, where limitations in the models used are most apparent. Results are presented in Fig. 10 and the fitted parameters listed in Table 7. When performing the fit for measurements at 30 °C, it was obvious that the lowest measurement point was out of reach of the simple models provided with the tool. To overcome the issue and to obtain a sensible fit, the first measurement point at 30 °C was, therefore, omitted as an outlier. To include such low current densities more detailed alkaline modelling should be employed. The number of measured data points was lower at 60 °C and the current density was not measured as low as for 30 °C. As the measurements did not include these very low current densities the fitting accuracy was greatly improved.

Despite the issue of imperfect models, both fitting methods performed well with the available data, producing consistent results within the error margins. As the number of measurements for 60 °C was quite low, the fit accuracy most likely exhibits phenomena presented in more detail in Section Measurement data quality.

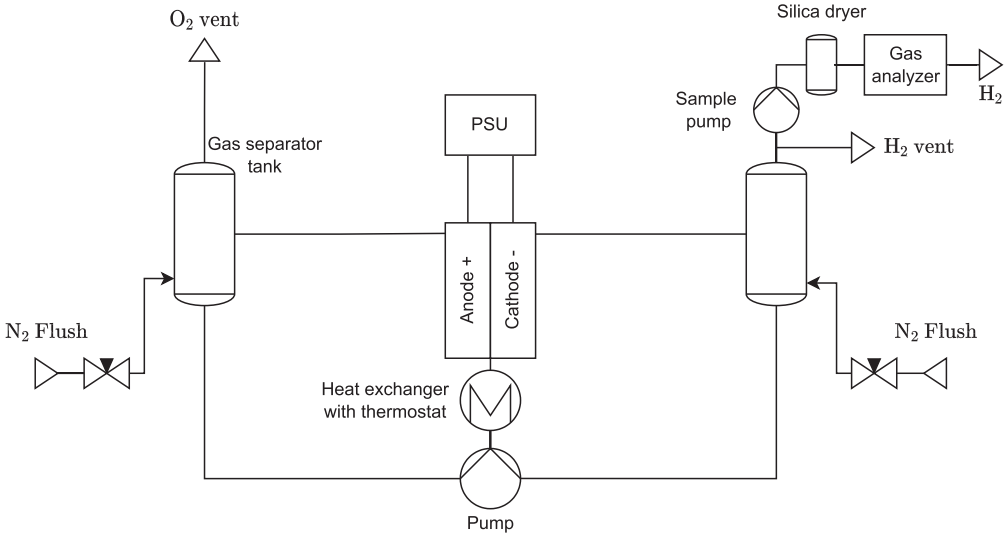

Fig. 8 – Simplified P&I diagram of the Alkaline test setup.

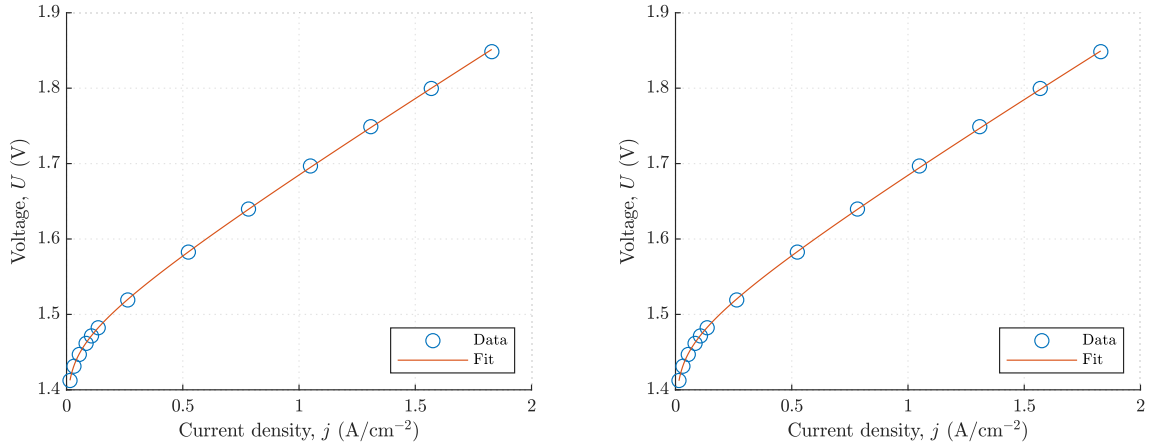

(a) Non-Linear Least Squares Estimation (b) Particle swarm

Fig. 9 – PEMWE current-voltage data fitted using the modelling tool.

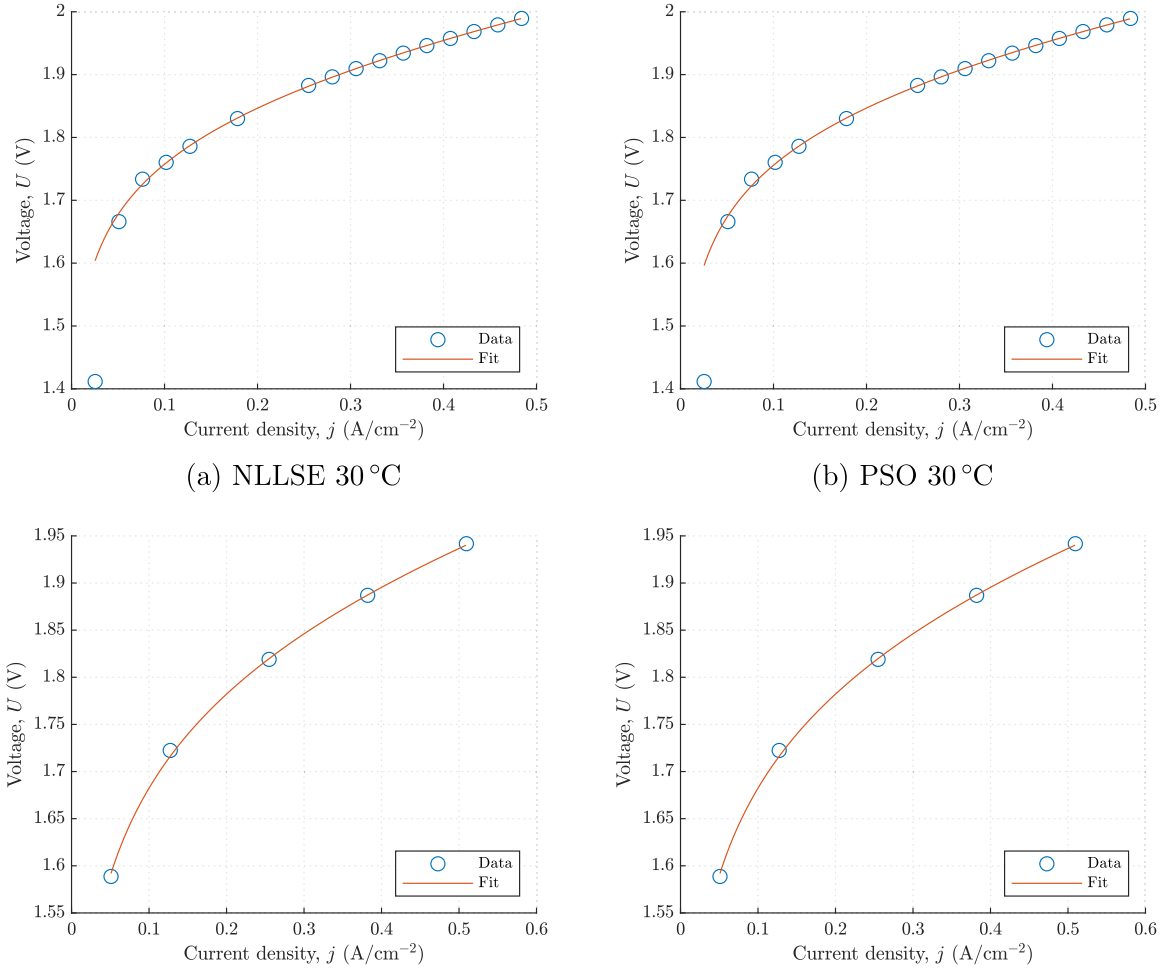

(a) NLLSE 30 °C (b) PSO 30 °C

(c) NLLSE 60 °C (d) PSO 60 °C

Fig. 10 – Light Bridge AWE current-voltage data fitted using the modelling tool.

Table 6 – Fit parameters and their standard deviations for the PEMWE current-voltage data.

Method	T	r ($\Omega\,cm^2$)	α (1)	j_0 (10^{-7} A cm^{-2})
NLLSE	75 °C	0.1853 ± 0.0010	0.703 ± 0.014	3.0 ± 0.7
PSO	75 °C	0.1830 ± 0.0007	0.685 ± 0.008	4.1 ± 0.6

Table 7 – Fit parameters and their standard deviations for Light Bridge AWE.

Method	T	r ($\Omega\,cm^2$)	α (1)	j_0 (10^{-4} A cm^{-2})
NLLSE	30 °C	0.186 ± 0.013	0.128 ± 0.004	6.4 ± 1.0
PSO	30 °C	0.17 ± 0.03	0.122 ± 0.006	8 ± 2
NLLSE	60 °C	0.13 ± 0.08	0.11 ± 0.02	22 ± 12
PSO	60 °C	0.13 ± 0.04	0.114 ± 0.006	23 ± 5

Measurement data quality

When measuring polarisation curves from real-world water electrolyzers, the data produced is never ideal. Examination of fitting for non-ideal data is thus important to be able to gauge the performance of the parameterizing capabilities of the tool and to look at cases where accuracy could be improved by additional measurements.

First, a sparse data set with a low number of measurement points was compared to a dense data set to see how much of a decrease in accuracy can be seen in the fit. Then, testing was done using data sets with missing low or high current densities. The missing data is generally caused by limitations in the electrolyzer under test or are a result of the test system power delivery limiting the polarisation curve measurement range, thus excluding activation or concentration overpotential dominated operation areas from the data.

Each test provides the average of the fitting error from a group of 10 synthetical measurements generated by the toolbox. Synthetical data was used to determine the limitations of the toolbox, as it provided a simple way to generate measurement data with a varied number of measurement points and allowed testing with a wide current density range. Additionally, using known parameters for the synthetical data allowed straightforward validation of the fitting accuracy, as the results from the fits could be compared to the original

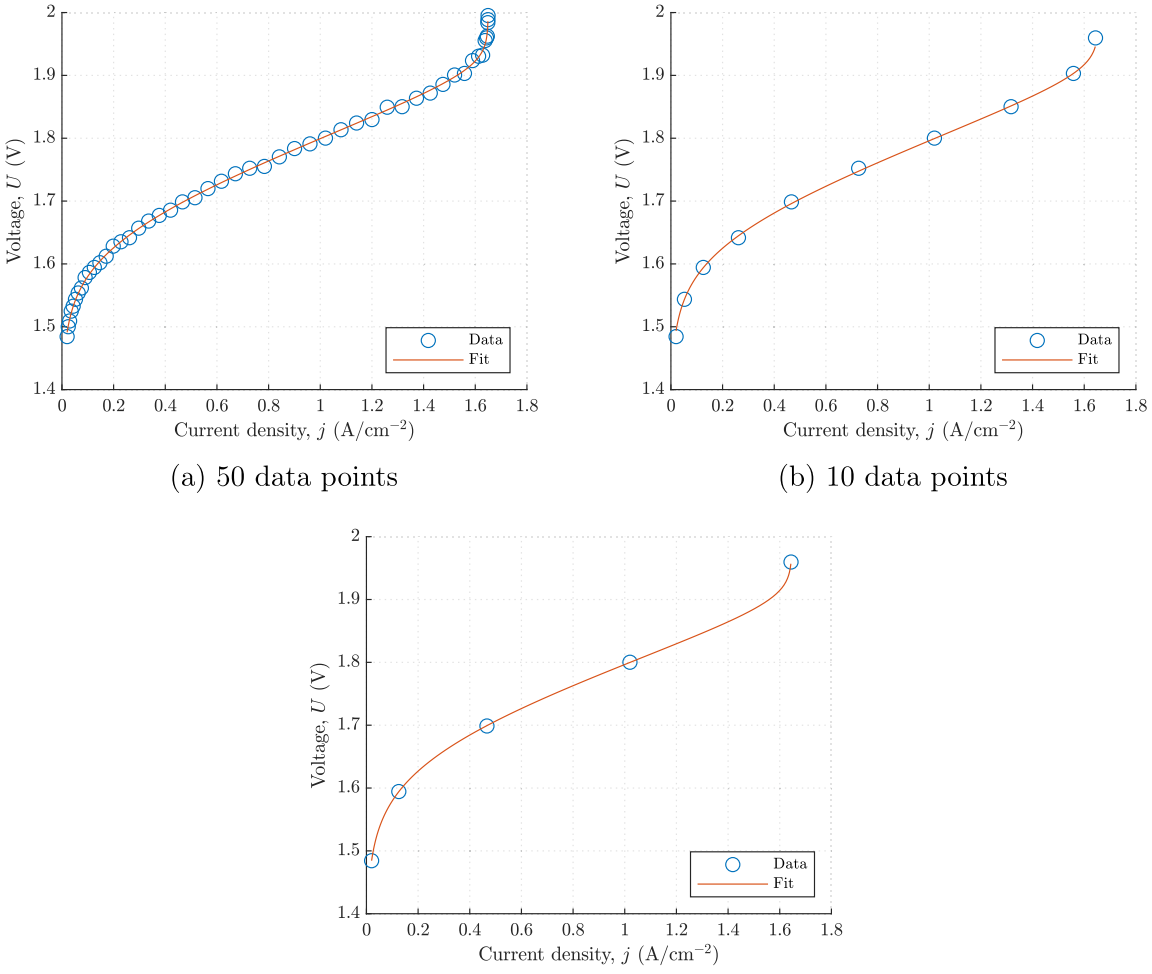

(a) 50 data points

(b) 10 data points

(c) 5 data points

Fig. 11 – Fitting performance compared between synthetic data sets of 50, 10 and 5 data points for the NLLSE fitting method.

values used to generate the data. The data was used to determine cases where more measurements are necessary to produce a fit with suitably accurate parameters for modelling.

Fitting performance was tested with three synthetic data sets of variable measurement density (50, 10 and 5 data points) to see the performance difference with non-optimal measurement data. Data was synthesized for a PEM water electrolyzer with the following parameters: $\alpha = 0.3$, $j_0 = 1.3 \times 10^{-4}$ A cm^{-2}, $r = 0.1\ \Omega\ \text{cm}^2$ and $j_{\text{lim}} = 1.65$ A cm^{-2}. Toolbox default models were used both for the open circuit voltage and for the overpotentials. Temperature was set to 353.15 K, and the cathode and anode pressures were 20 bar and 2 bar, respectively. Sparser data sets were created by picking evenly spaced observations from the dense data to avoid wide difference in their measurement errors.

The fitted polarisation curves are illustrated in Fig. 11 and the fit parameters, which are averaged over the ten sets are presented for each fitting method and measurement point density in Table 8. As the resulting plots from PSO were nearly identical and not separable from those obtained from NLLSE, only the latter are presented in the figures. Both fitting methods work well with both the dense and sparse data sets as can be seen from the fitted parameters, which show little difference between the different cases.

As expected, fittings created using the sparser data set produce more error compared to the results from the dense data set.

Finally, fitting performance was tested with two synthetic data sets where low or high current densities were missing. Operation and measurement range limitations are quite common in measurement systems, and they can affect the accuracy of the fittings. The tests were done to show the effects of such missing data.

The same synthetic data and fitting procedures were used as in the measurement density tests. The data sets were then created by considering only the first 3/4 of the measurement points for low current density measurements, and only the last 3/4 of the data points for high current density measurements. The fitted polarisation curves are illustrated in Fig. 12 and the fit parameters averaged over the ten sets for each method and measurement point density are listed in Table 9. As the resulting plots from the two methods were again non-separable, only those obtained from NLLSE are presented.

As can be expected, the activation phenomena are better observed from the low current densities, whereas the limiting current density is observable only when the measurement range covers high enough current densities. The electron transfer coefficient α and exchange current density j_0 have higher error bounds with data that has limited range on low current density, while the accuracy of limiting current density j_{lim} suffers when high current densities are missing. The resistance value is best evaluated from the middle portion of the polarisation curve and therefore seems to be unsensitive to the change in the measurement range.

Table 8 – Fit parameters and their standard deviations for synthetic data sets of 50, 10 and 5 data points. The values are a mean of the parameters for 10 independent data sets of the respective kind.

Method, n	r ($\Omega\,\text{cm}^2$)	α (1)	j_0 (10^{-4} A cm^{-2})	j_{lim} (A cm^{-2})
true values	0.1	0.3	1.3	1.65
NLLSE, 50	0.099 ± 0.002	0.300 ± 0.006	1.31 ± 0.14	1.650 00 ± 0.000 07
NLLSE, 10	0.101 ± 0.007	0.302 ± 0.014	1.2 ± 0.4	1.650 ± 0.003
NLLSE, 5	0.1 ± 0.3	0.3 ± 0.3	1 ± 7	1.65 ± 0.14
PSO, 50	0.099 ± 0.002	0.298 ± 0.006	1.35 ± 0.15	1.650 00 ± 0.000 10
PSO, 10	0.101 ± 0.004	0.305 ± 0.008	1.3 ± 0.3	1.650 ± 0.002
PSO, 5	0.102 ± 0.005	0.305 ± 0.008	1.2 ± 0.2	1.652 ± 0.004

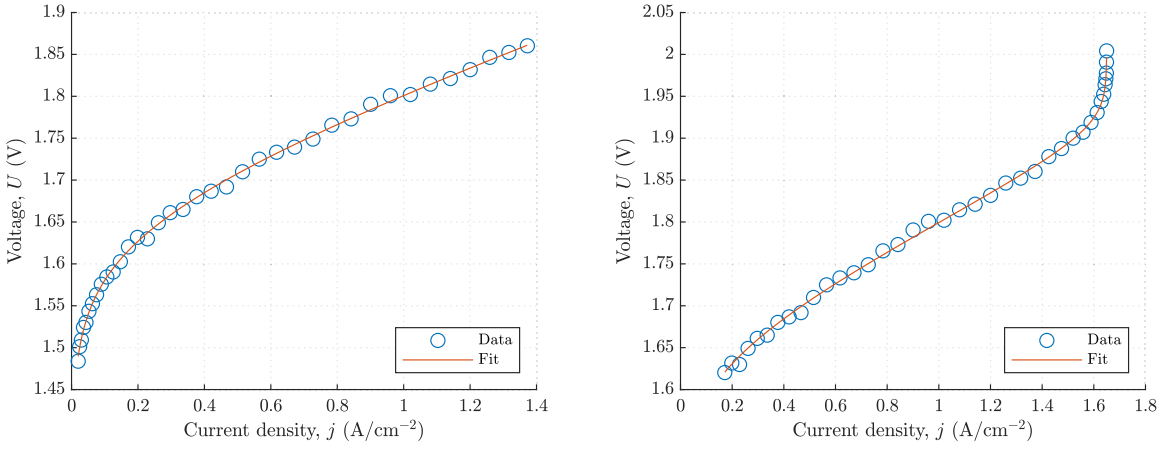

(a) Low NLLSE data (b) High NLLSE data

Fig. 12 – Fitting performance compared between data sets which have low or high current densities missing.

Table 9 – Fit parameters and their standard deviations for synthetic data sets with only the lower or higher three quarters of the data. The values are a mean of the parameters for 10 independent data sets of the respective kind.

Method, range	r ($\Omega\,cm^2$)	α (1)	j_0 (10^{-4} A cm^{-2})	j_{lim} (A cm^{-2})
true values	0.1	0.3	1.3	1.65
NLLSE, low	0.101 ± 0.008	0.298 ± 0.007	1.4 ± 0.2	2 ± 2
NLLSE, high	0.101 ± 0.005	0.31 ± 0.02	1.2 ± 0.6	1.650 00 ± 0.000 07
PSO, low	0.099 ± 0.007	0.299 ± 0.007	1.4 ± 0.2	1.7 ± 0.6
PSO, high	0.101 ± 0.004	0.31 ± 0.02	1.4 ± 0.6	1.650 00 ± 0.000 11

Conclusion

A tool for simplifying proton exchange membrane water electrolyzer (PEMWE) and alkaline water electrolyzer (AWE) modelling and parametrization was developed in this work. The aim was to provide a standardized way of modelling water electrolyzer systems and to provide much simpler workflow for polarisation curve parameterization. The tooling was verified with data from a PEMWE provided by Forschungszentrum Jülich, Germany, and AWE data from LUT University, Finland.

Commonly used analytical and empirical water electrolyzer voltage models have been gathered and implemented into an easy-to-use MATLAB toolbox. Multiple models for each overpotential are included and as this kind of tool is only as good as the models themselves, considerable emphasis has been placed on making the tool modular so that adding additional models is easy. The parameterization component of the tool implements fitting using the Non-Linear Least Square Error regression (NLLSE) method and Particle Swarm Optimisation (PSO). All the code for the tooling is going to be released as open-source code under a BSD 3-Clause licence and the toolbox is going to be published in file exchange at MATLAB Central with the name "Electrolyzer modelling toolbox".

Results from parametrization of the PEMWE and AWE showed limitations in the current overpotential models. For state-of-the-art PEMWE, the parameters obtained via fitting are well in line with numbers provided in literature and the resulting fit characterizes the system well. On the other hand, the activation overpotentials of the AWE could not be fitted properly due to limitations in the model used. The limitations in the models caused high error in the fit, and as such the low current measurement point had to be omitted for 30 °C measurements. Very similar performance was seen from both the NLLSE and PSO fitting methods.

Looking at the results from non-optimal data sets where the measurement point density and range was varied, it can be seen that having a small number of data points does not seem to affect the resulting fit from PSO significantly, even with only five evenly spaced data points the error margins for PSO fitting are close to those provided by fits produced for the 50-point data set. The NLLSE method struggles much more with low density data sets, which cause parameters to have higher error margins than the value itself, making this method very unreliable for low data density fitting. Both methods performed almost identically when using data that is missing either low current densities or higher current densities,. If low current densities have not been measured, the electron transfer coefficient and the current exchange density both have high error margins as the parameters affect the low current portion of the polarisation curve and cannot be fitted well when these measurement points are missing. On the other hand, the limiting current density only has an effect on high current densities which makes its parametrization very difficult when high current densities are fitted.

The tooling works with a wide variety of use cases and provides a much more straight forward way of modelling and parameterizing water electrolyzer polarisation curves than is otherwise available. The included error checking ensures that the limitations of the different models are taken into account reducing the number of easily preventable mistakes.

At this point, the model bank only incorporates the most popular models for calculating the reversible potential and the overpotentials. Limitations with taking into consideration the temperature change have already been identified in the activation and ohmic overpotential models, which limit the prediction capabilities of the models. Additionally more accurate gas models of the electrolyzer systems which include gas crossovers need to be implemented in the future. Expanding the modelling bank with more accurate models is one of the areas requiring improvement.

Development is also needed to implement models that consider dynamic behaviour, as this would greatly help modelling efforts with variable power sources, like renewable energy. These models demand a significant increase in the model complexity by requiring solving of ordinary differential and partial differential equations.

The results in this study show that the tool can be used with different electrolyzers to perform parametrization and polarisation curve modelling with accurate results. Limitations in commonly used electrolyzer models presents an opportunity for further development to increase accuracy and expand the use cases of the tool even further.

Declaration of competing interest

The authors declare that they have no known competing financial interests or personal relationships that could have appeared to influence the work reported in this paper.

Acknowledgement

The Academy of Finland is acknowledged for the main financial support of the Research of Power Quality Effect on Water Electrolyzer Operation (POQELYZER) project.

REFERENCES

[1] UNFCCC. The Paris agreement. In: Paris climate change conference. Paris: UNFCCC; 2015.
[2] Falcão DS. A review on PEM electrolyzer modelling: guidelines for beginners. J Clean Prod 2020:10.
[3] Hernández-Gómez Á, Ramirez V, Guilbert D. Investigation of PEM electrolyzer modeling: electrical domain, efficiency, and specific energy consumption. Int J Hydrogen Energy 2020;45(29):14625–39. https://doi.org/10.1016/j.ijhydene.2020.03.195.
[4] Olivier P, Bourasseau C, Bouamama PB. Low-temperature electrolysis system modelling: a review. Renew Sustain Energy Rev 2017;78:280–300. https://doi.org/10.1016/j.rser.2017.03.099.
[5] Gambou F, Guilbert D, Zasadzinski M, Rafaralahy H. A comprehensive survey of alkaline electrolyzer modeling: electrical domain and specific electrolyte conductivity. Energies 2022;15(9):3452. https://doi.org/10.3390/en15093452.
[6] Abdin Z, Webb C, Gray E. Modelling and simulation of a proton exchange membrane (PEM) electrolyser cell. Int J Hydrogen Energy 2015;40(39):13243–57. https://doi.org/10.1016/j.ijhydene.2015.07.129.
[7] Correa G, Marocco P, Muñoz P, Falagüerra T, Ferrero D, Santarelli M. Pressurized PEM water electrolysis: dynamic modelling focusing on the cathode side. Int J Hydrogen Energy 2022;47(7):4315–27. https://doi.org/10.1016/j.ijhydene.2021.11.097.
[8] Choi P, Bessarabov DG, Datta R. A simple model for solid polymer electrolyte (SPE) water electrolysis. Solid State Ionics 2004;175(1):535–9. https://doi.org/10.1016/j.ssi.2004.01.076.
[9] García-Valverde R, Espinosa N, Urbina A. Simple PEM water electrolyser model and experimental validation. Int J Hydrogen Energy 2012;37(2):1927–38. https://doi.org/10.1016/j.ijhydene.2011.09.027.
[10] Hammoudi M, Henao C, Agbossou K, Dubé Y, Doumbia ML. New multi-physics approach for modelling and design of alkaline electrolyzers. Int J Hydrogen Energy 2012;37(19):13895–913. https://doi.org/10.1016/j.ijhydene.2012.07.015.
[11] Henao C, Agbossou K, Hammoudi M, Dubé Y, Cardenas A. Simulation tool based on a physics model and an electrical analogy for an alkaline electrolyser. J Power Sources 2014;250:58–67. https://doi.org/10.1016/j.jpowsour.2013.10.086.
[12] Koponen J, Ruuskanen V, Hehemann M, Rauls E, Kosonen A, Ahola J, Stolten D. Effect of power quality on the design of proton exchange membrane water electrolysis systems. Appl Energy 2020;279:115791. https://doi.org/10.1016/j.apenergy.2020.115791.
[13] Dale NV, Mann MD, Salehfar H. Semiempirical model based on thermodynamic principles for determining 6kW proton exchange membrane electrolyzer stack characteristics. J Power Sources 2008;185(2):1348–53. https://doi.org/10.1016/j.jpowsour.2008.08.054.
[14] Ulleberg O. Modeling of advanced alkaline electrolyzers: a system simulation approach. Int J Hydrogen Energy 2003;28(1):21–33. https://doi.org/10.1016/S0360-3199(02)00033-2.
[15] Sakas G, Ibáñez-Rioja A, Ruuskanen V, Kosonen A, Ahola J, Bergmann O. Dynamic energy and mass balance model for an industrial alkaline water electrolyzer plant process. Int J Hydrogen Energy 2022;47(7):4328–45. https://doi.org/10.1016/j.ijhydene.2021.11.126.
[16] Brée LC, Schiekel T, Mitsos A. Overpotentials in water electrolysis: in-silico comparison of PEM-cell and GAP-cell performance. In: Computer aided chemical engineering. 46. Elsevier; 2019. p. 847–52. https://doi.org/10.1016/B978-0-12-818634-3.50142-9.
[17] Onda K, Murakami T, Hikosaka T, Kobayashi M, Notu R, Ito K. Performance analysis of polymer-electrolyte water electrolysis cell at a small-unit test cell and performance prediction of large stacked cell. J Electrochem Soc 2002;149(8):A1069. https://doi.org/10.1149/1.1492287.
[18] Chandesris M, Médeau V, Guillet N, Chelghoum S, Thoby D, Fouda-Onana F. Membrane degradation in PEM water electrolyzer: numerical modeling and experimental evidence of the influence of temperature and current density. Int J Hydrogen Energy 2015;40(3):1353–66. https://doi.org/10.1016/j.ijhydene.2014.11.111.
[19] Ma Z, Witteman L, Wrubel JA, Bender G. A comprehensive modeling method for proton exchange membrane electrolyzer development. Int J Hydrogen Energy 2021;46(34):17627–43. https://doi.org/10.1016/j.ijhydene.2021.02.170.
[20] Ursúa A, Sanchis P. Static–dynamic modelling of the electrical behaviour of a commercial advanced alkaline water electrolyser. Int J Hydrogen Energy 2012;37(24):18598–614. https://doi.org/10.1016/j.ijhydene.2012.09.125.
[21] Ursua A, Gandia LM, Sanchis P. Hydrogen production from water electrolysis: current status and future trends. Proc IEEE 2012;100(2):410–26. https://doi.org/10.1109/JPROC.2011.2156750.
[22] Schalenbach M, Tjarks G, Carmo M, Lueke W, Mueller M, Stolten D. Acidic or alkaline? Towards a new perspective on the efficiency of water electrolysis. J Electrochem Soc 2016;163(11):F3197. https://doi.org/10.1149/2.0271611jes.
[23] Rumble JR. Electrochemical series. In: CRC handbook of chemistry and physics, one hundred second edition. Boca Raton, FL: CRC Press/Taylor & Francis; 2021 (Internet Version).
[24] LeRoy RL, Bowen CT, LeRoy DJ. The thermodynamics of aqueous water electrolysis. J Electrochem Soc 1980;127(9):1954. https://doi.org/10.1149/1.2130044.
[25] Bernardi DM, Verbrugge MW. A mathematical model of the solid-polymer-electrolyte fuel cell. J Electrochem Soc 1992;139(9):2477–91. https://doi.org/10.1149/1.2221251.
[26] Schalenbach M. Proton conduction and gas permeation through polymer electrolyte membranes during water electrolysis. RWTH Aachen University, Forschungszentrum Jülich GmbH; 2018. Ph.D. thesis.
[27] da Costa Lopes F, Watanabe EH. Experimental and theoretical development of a PEM electrolyzer model applied to energy storage systems, in: 2009 Brazilian power electronics conference. 2009. p. 775–82. https://doi.org/10.1109/COBEP.2009.5347619.
[28] Han B, Steen SM, Mo J, Zhang F-Y. Electrochemical performance modeling of a proton exchange membrane electrolyzer cell for hydrogen energy. Int J Hydrogen Energy 2015;40(22):7006–16. https://doi.org/10.1016/j.ijhydene.2015.03.164.
[29] Biaku CY, Dale NV, Mann MD, Salehfar H, Peters AJ, Han T. A semiempirical study of the temperature dependence of the anode charge transfer coefficient of a 6kW PEM electrolyzer. Int J Hydrogen Energy 2008;33(16):4247–54. https://doi.org/10.1016/j.ijhydene.2008.06.006.
[30] Bridgeman OC, Aldrich EW. Vapor pressure tables for water. J Heat Tran 1964;86(2):279–86. https://doi.org/10.1115/1.3687121.
[31] Balej J. Water vapour partial pressures and water activities in potassium and sodium hydroxide solutions over wide concentration and temperature ranges. Int J Hydrogen Energy 1985;10(4):233–43.

[32] Noren DA, Hoffman MA. Clarifying the Butler–Volmer equation and related approximations for calculating activation losses in solid oxide fuel cell models. J Power Sources 2005;152:175–81. https://doi.org/10.1016/j.jpowsour.2005.03.174.
[33] Bard AJ, Faulkner LR. Electrochemical methods: fundamentals and applications. 2nd ed. John Wiley & Sons; 2000.
[34] Thampan T, Malhotra S, Zhang J, Datta R. PEM fuel cell as a membrane reactor. Catal Today 2001;67(1):15–32. https://doi.org/10.1016/S0920-5861(01)00278-4.
[35] Nie J, Chen Y, Boehm RF, Katukota S. A photoelectrochemical model of proton exchange water electrolysis for hydrogen production. J Heat Tran 4) (Mar. 2008;130. https://doi.org/10.1115/1.2789722.
[36] Kai J, Saito R, Terabaru K, Li H, Nakajima H, Ito K. Effect of temperature on the performance of polymer electrolyte membrane water electrolysis: numerical analysis of electrolysis voltage considering gas/liquid two-phase flow. J Electrochem Soc 2019;166(4):F246. https://doi.org/10.1149/2.0521904jes.
[37] Ni M, Leung MKH, Leung DYC. Energy and exergy analysis of hydrogen production by a proton exchange membrane (PEM) electrolyzer plant. Energy Convers Manag 2008;49(10):2748–56. https://doi.org/10.1016/j.enconman.2008.03.018.
[38] Ruuskanen V, Koponen J, Kosonen A, Hehemann M, Keller R, Niemelä M, Ahola J. Power quality estimation of water electrolyzers based on current and voltage measurements. J Power Sources 2020;450:227603. https://doi.org/10.1016/j.jpowsour.2019.227603.
[39] Sheng W, Gasteiger HA, Shao-Horn Y. Hydrogen oxidation and evolution reaction kinetics on platinum: acid vs alkaline electrolytes. J Electrochem Soc 2010;157(11):B1529. https://doi.org/10.1149/1.3483106.
[40] Marangio F, Santarelli M, Calì M. Theoretical model and experimental analysis of a high pressure PEM water electrolyser for hydrogen production. Int J Hydrogen Energy 2009;34(3):1143–58. https://doi.org/10.1016/j.ijhydene.2008.11.083.
[41] Saeed EW, Warkozek EG. Modeling and analysis of renewable PEM fuel cell system. Energy Proc 2015;74:87–101. https://doi.org/10.1016/j.egypro.2015.07.527.
[42] Nafeh AE-SA. Hydrogen production from a PV/PEM electrolyzer system using a neural-network-based MPPT algorithm. Int J Numer Model Electron Network Dev Field 2011;24(3):282–97. https://doi.org/10.1002/jnm.778.
[43] Lebbal M, Lecœuche S. Identification and monitoring of a PEM electrolyser based on dynamical modelling. Int J Hydrogen Energy 2009;34(14):5992–9. https://doi.org/10.1016/j.ijhydene.2009.02.003.
[44] Shinagawa T, Garcia-Esparza AT, Takanabe K. Insight on Tafel slopes from a microkinetic analysis of aqueous electrocatalysis for energy conversion. Sci Rep 2015;5(1):13801. https://doi.org/10.1038/srep13801.
[45] Chen Y, Mojica F, Li G, Chuang P-YA. Experimental study and analytical modeling of an alkaline water electrolysis cell. Int J Energy Res 2017;41(14):2365–73. https://doi.org/10.1002/er.3806.
[46] Bernardi DM, Verbrugge MW. Mathematical model of a gas diffusion electrode bonded to a polymer electrolyte. AIChE J 1991;37(8):1151–63. https://doi.org/10.1002/aic.690370805.
[47] Springer TE, Zawodzinski TA, Gottesfeld S. Polymer electrolyte fuel cell model. J Electrochem Soc 1991;138(8):2334. https://doi.org/10.1149/1.2085971.
[48] Gilliam R, Graydon J, Kirk D, Thorpe S. A review of specific conductivities of potassium hydroxide solutions for various concentrations and temperatures. Int J Hydrogen Energy 2007;32(3):359–64. https://doi.org/10.1016/j.ijhydene.2006.10.062.
[49] See DM, White RE. Temperature and concentration dependence of the specific conductivity of concentrated solutions of potassium hydroxide. J Chem Eng Data 1997;42(6):1266–8. https://doi.org/10.1021/je970140x.
[50] Le Bideau D, Mandin P, Benbouzid M, Kim M, Sellier M. Review of necessary thermophysical properties and their sensivities with temperature and electrolyte mass fractions for alkaline water electrolysis multiphysics modelling. Int J Hydrogen Energy 2019;44(10):4553–69. https://doi.org/10.1016/j.ijhydene.2018.12.222. see Corrigendum.
[51] Zaytsev ID, Aseyev GG. Properties of aqueous solutions of electrolytes. CRC Press; 1992.
[52] Piotrowski AP, Napiorkowski JJ, Piotrowska AE. Population size in particle swarm optimization. Swarm Evol Comput 2020;58:100718. https://doi.org/10.1016/j.swevo.2020.100718.
[53] Laine M. MCMC toolbox for Matlab. Aug. 2021.
[54] Stähler M, Stähler A, Scheepers F, Carmo M, Stolten D. A completely slot die coated membrane electrode assembly. Int J Hydrogen Energy 2019;44(14):7053–8. https://doi.org/10.1016/j.ijhydene.2019.02.016.